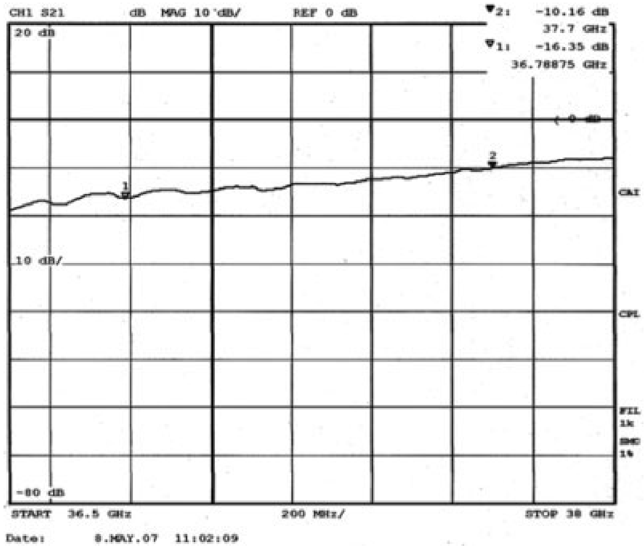

Figure 5 Isolation in unbiased state of the balanced BPSK modulator

A wave incident on the finline is phase shifted by 180 ° that is the orientation of the electric field in the coplanar line is switched when the position of the short is exchanged as shown in Figure 1. The 180 ° phase shift is independent of frequency, in spite of changes in characteristics because of frequency-dependent elements of the actual circuit like length of the coplanar line section which adds to the mismatch.

4. EXPERIMENTAL TEST RESULTS

Figures 3 and 4 shows the measured results of the balanced phase modulator. The amplitude in the two states is shown in Figure 3. An insertion loss imbalance of $\pm$1.5 dB with an average loss of 2.5 dB in the two switching states has been achieved over 37.0–38.0 GHz. The phase difference between the two states is shown in Figure 4. The phase imbalance is $\pm 10°$ with phase switching from 165° to 185°. Figure 5 shows the Isolation in the unbiased state.

5. CONCLUSION

The designed BPSK modulators have high isolation between the carrier input port and the modulated carrier output port. The pulse width variations and amplitude deviations are suppressed because of the balanced configuration used. As the PSK output signal is in Suspended Stripline, Two BPSK Modulators can easily be combined together to work as QPSK Modulator for point to point Millimeter Wave Radio Links [4]. These modulators will enable compact, low-cost, and high-efficiency transmitters for millimeter wave digital communication systems.

REFERENCES

1. C.H.H. Meinel and W.J.R. Hoefer, p-i-n diode control devices in E-plane technique, IEEE MTT-37 2 (1989), 307–316.
2. R. Sato, Transmission circuit, Corna, Tokyo, 1973, pp. 43–47.
3. B. Bhat and S.K. Koul, Analysis, design and applications of fin lines, Artech House, MA, 1987.
4. B. Jokanovic, S. Stojanovic, and M. Peric, Direct QPSK modulator for point-to-point radio link at 23 GHz, 5th International Conference on Telecommunications in Modern Satellite, Cable and Broadcasting Service TELSIKS 2001. pp. 217–220.

OPTIMIZATION OF INTEGRATED CIRCUITS PLACEMENT FOR ELECTRIC FIELD REDUCTION INSIDE TELECOMMUNICATIONS EQUIPMENT USING MONTE CARLO SIMULATION AND PARALLEL RECOMBINATIVE SIMULATED ANNEALING

Sotirios K. Goudos,[1] Zaharias D. Zaharis,[1,2] Pavlos I. Lazaridis,[2,3] and Philippe B. Gallion[3]
[1] Telecommunications Centre, Aristotle University of Thessaloniki, 54124 Thessaloniki, Greece; Corresponding author: zaharis@auth.gr
[2] Department of Electronics, Alexander Technological Educational Institute of Thessaloniki, 57400 Thessaloniki, Greece
[3] Département Communications et Electronique, Unité de Recherche Associée au Centre National de la Recherche Scientifique, 820 Ecole Nationale Supérieure des Télécommunications, 46 Rue Barrault, 75634 Paris Cedex 13, France

Received 15 May 2007

ABSTRACT: *This article presents a novel approach to the modeling and reduction of electromagnetic interference (EMI) caused by radiated emissions of integrated circuits (ICs) inside rectangular metallic enclosures of telecommunications devices. This type of analysis applies for several types of modern telecommunications equipment found in high-speed networks as well as in mobile communications. A generic model of such a device is created. The ICs are modeled as small electric dipoles and their interaction with the enclosure walls is studied by using the dyadic Green's functions. The electric field on the enclosure walls is computed and its reduction is studied as optimization problem using evolutionary algorithms. Two algorithms are employed: Genetic algorithms (GAs) and parallel recombinative simulated annealing (PRSA). PRSA is a hybrid evolutionary strategy that inherits properties from both GAs and simulated annealing. Monte Carlo simulation is subsequently applied to the optimization results to derive the electric field on the metallic walls and also to perform a worst-case analysis. The applications of the above approach in early PCB design process are discussed.* © 2007 Wiley Periodicals, Inc. Microwave Opt Technol Lett 49: 3049–3055, 2007; Published online in Wiley InterScience (www.interscience.wiley.com). DOI 10.1002/mop.22893

Key words: *electromagnetic compatibility; Monte Carlo simulation; Green's functions calculation; genetic algorithms; simulated annealing; parallel programming*

1. INTRODUCTION

New technologies in telecommunications and computer industry are constantly emerging. Modern devices manufactured for wired and wireless communications include integrated circuits (ICs) with faster clock speeds. Motherboards and other PCBs (printed circuit boards) become more complex. The fundamentals of microwave communications can be found in several textbooks [1-3]. The problem of predicting EMI (electromagnetic interference) levels and complying with regulatory EMC standards is very common [4, 5]. It is advantageous to be able to make estimation for the EMI potential from PCBs during the design process. The correct placement of ICs on PCBs inside a shielded enclosure has an effect on the interference issue. Radiated emissions from PCBs have been studied extensively in several papers [6-10]. Electromagnetic penetration inside a metallic cavity with or without slots is also a common issue [11-15]. In all previous work, numerical or analytical deterministic methods are used for EMI calculation. In this article, a novel stochastic method combined with evolutionary optimization algorithms is proposed.

The ICs can be modeled as small electric and magnetic current sources. The interaction between cavity walls and internal dipoles can be described by using the dyadic Green's functions [16]. The mapping matrix approach is subsequently applied [17-19]. This approach outlines the interaction inside the enclosure between the metallic walls and the small dipole sources. The method for measuring radiated emissions from ICs is described in [20, 21]. The validity of this modeling has been verified after suitable characterizations and measurements of several telecommunications equipment devices found in high-speed networks as well as in mobile communications. The effect of magnetic dipole sources that induce surface current density has been already studied in [18, 19].

In this article, the electric field induced on the walls of a metallic rectangular enclosure due to electric dipole sources for several positions and directions of the sources is presented. The problem of reducing EMI on the enclosure walls is solved using genetic algorithms (GAs) [22] and parallel recombinative simulated annealing (PRSA) [23]. PRSA is an evolutionary algorithm that uses basic concepts and operators from both GAs (crossover, mutation, parallel populations) and simulated annealing (temperature drop). PRSA has been successfully applied in several engineering design problems [24-26]. To the best of the authors' knowledge, this is the first time that PRSA is used in an electromagnetics design problem.

For the numerical investigation of the induced field, Monte Carlo simulation is employed in optimization results using both source existence and source phase probabilistic distributions. This article is organized as follows: Section 2 presents the formulation with closed form expressions. Section 3 shows numerical results of the electric field induced on the walls of a generic telecommunications equipment model. Section 4 presents the Monte Carlo simulation details. The optimization problem is defined in Section 5 and the algorithm details and results are given. Finally, the conclusions are summarized in Section 6.

2. FORMULATION

For the rectangular cavity with dimensions a, b, and c, ($a = c = L$, $b = 0.3L$), along x, y, and z-axis, respectively (see Fig. 1), the expressions for the dyadic Green's function of the magnetic and electric vector potential are given in [16-18]. A detailed description of the relation between the magnetic and electric dipole sources placed inside the cavity and the surface current density induced on the cavity walls is given in [18, 19]. The electric and magnetic field induced inside the cavity by a small electric dipole with current density $\bar{J}_e(\bar{r}')$ are given by

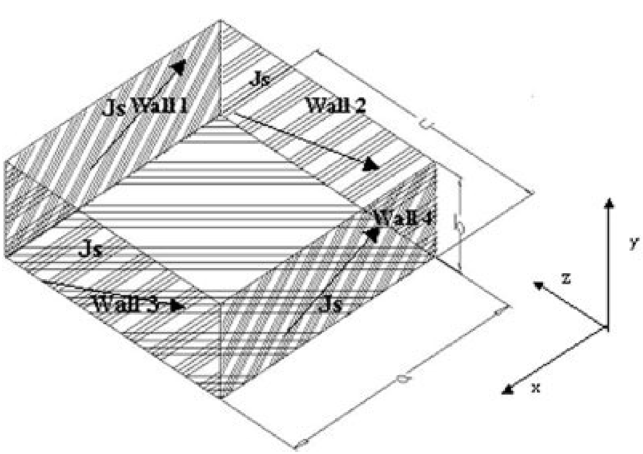

Figure 1 Rectangular enclosure geometry ($a = c = L$, $b = 0.3L$)

$$\bar{E}^e(\bar{r}) = \int_{V'} \bar{\bar{G}}_e(\bar{r}|\bar{r}')\,\bar{J}_e(\bar{r}')dV', \tag{1}$$

$$\bar{H}^e(\bar{r}) = \frac{1}{j\omega\mu_o}\int_{V'} \bar{\bar{G}}_h(\bar{r}|\bar{r}')\,\bar{J}_e(\bar{r}')dV', \tag{2}$$

where $\bar{r}$ and $\bar{r}'$ are the position vectors of the field and the source point, , respectively, V' is the source volume over which the current density is distributed, and finally $\bar{\bar{G}}_e$ and $\bar{\bar{G}}_h$ are the dyadic Green's functions for the E and H fields due to an electric dipole source inside a rectangular cavity.

The closed form expressions for the induced electric field on the $z = c$ wall (for $z > z'$) due to the electric dipole moments p_x, p_y, p_z are given by

$$\bar{E} = \frac{p_x}{ab}\sum_m\sum_n e_m e_n \frac{k_x}{k^2}\left(\frac{\sin(k_g z')}{\sin(k_g c)}\right)\sin(k_x x)\sin(k_y y)\cos(k_x x')\sin(k_y y')\,\hat{z}, \tag{3}$$

$$\bar{E} = \frac{p_y}{ab}\sum_m\sum_n e_m e_n \frac{k_y}{k^2}\left(\frac{\sin(k_g z')}{\sin(k_g c)}\right)\sin(k_x x)\sin(k_y y)\sin(k_x x')\cos(k_y y')\,\hat{z}, \tag{4}$$

$$\bar{E} = -\frac{p_z}{ab}\sum_{ml}\sum_n e_m e_n \frac{k_c^2}{k^2}\left(\frac{\cos(k_g z')}{k_g\sin(k_g c)}\right)\sin(k_x x)\sin(k_y y)\sin(k_x x')\sin(k_y y')\,\hat{z}. \tag{5}$$

The coefficients in (3), (4), and (5) are given below:

$$k = \omega\sqrt{\mu_0\varepsilon_0} = \frac{2\pi}{\lambda},\ k_x = \frac{m\pi}{a},\ k_y = \frac{n\pi}{b},\ k_z = \frac{l\pi}{c},$$
$$k_c^2 = k_x^2 + k_y^2,\ k_g^2 = k^2 - k_c^2 \tag{6}$$

$$e_i = \begin{cases} 1 & i = 0 \\ 2 & i \neq 0 \end{cases}.$$

It is evident from (3), (4), and (5) that the induced electric filed depends on the cavity geometry on the source frequency (or wavelength) and on the electric dipole moment.

3. TELECOMMUNICATIONS EQUIPMENT MODEL

Various types of telecommunications equipment include multiple source systems within rectangular shielded enclosures. Multiple sources inside the rectangular cavity of Figure 1 are considered. In that case, if N possible cavity sources exist and M wall points of interest are taken into account then the amplitude mapping of every source to a specific point on the wall can be represented by an $N \times M$ matrix A [17, 18]. Matrix A is called mapping matrix. In A, a matrix element ρ_{ij} represents the disturbance on jth point caused by the ith source. Disturbances caused by multiple sources at the same reference wall point can be summed using the principle of superposition.

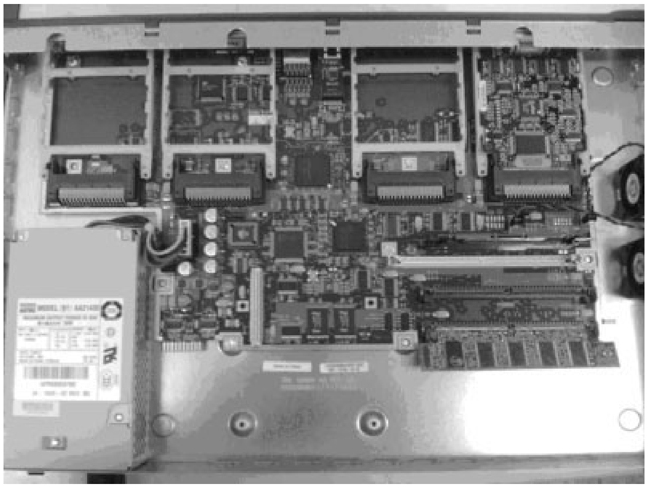

Figure 2 Photo of a typical telecommunications equipment board

In all the results, the sources are assumed to be placed near the bottom of the cavity at $y' = 0.05L$ for $L = 0.1\lambda$. It has been shown in [27] that the electric field component resulting from the electric dipoles parallel to x-axis presents an antisymmetric behavior. It is therefore of particular interest. This implies that the random source configurations could produce different results. This was the reason for selecting to study the above component in the following examples.

A photo of a typical telecommunications board is given in Figure 2. This type of board can be found in various telecommunications devices such as videoconference equipment, protocol gateways, VoIP software switches, routers and wireless access points. These kinds of equipment work at low CPU speeds below 100 MHz. An enclosure with the dimensions given in Figure 1 ($a = c = L$, $b = 0.3L$) is selected. A source model has been created using empirical rules derived from several different boards of telecommunications equipment. Figure 3 shows a typical telecommunications PCB model consisting of 34 sources. The board model is separated in eight distinct areas with different source number and different source existence probabilities. The details of the telecommunications board probabilistic model are given in Table 1. Each source is named using the convention $m \times n$, where m is the area number from 1 to 8 and n is the source number for that area. For example, source 51 corresponds to the first source in area 5. This model is suitable for most modern telecommunications equipment.

The electric field distribution on walls 1 and 4 of this board model due to electric dipoles parallel to x-axis is given in Figures

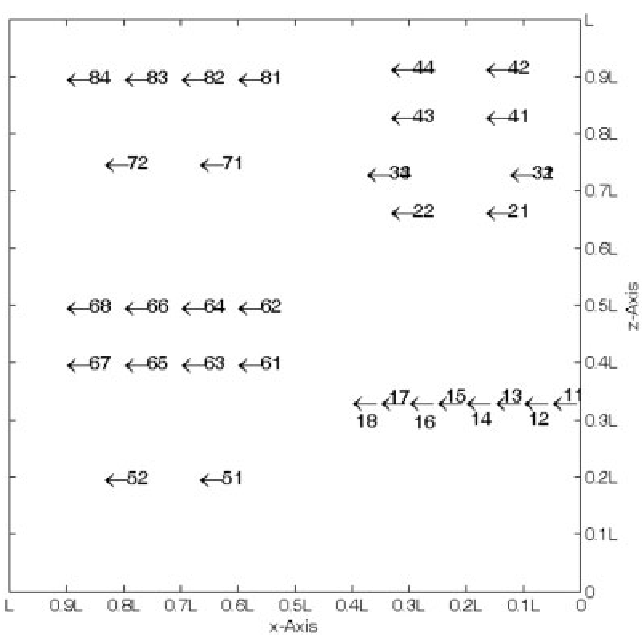

Figure 3 Telecommunications board source grid model

TABLE 1 Source Existence Probability Inside a Telecommunications Board Model

Area No.	Area	Maximum Source Number	Source Existence Probability
1	RAM	8	1
2	Chipset	2	0.5
3	CPU	4	0.7
4	Network Interface 1	4	0.5
5	ASIC 1	2	0.2
6	ASIC 2	8	0.6
7	Slots	2	0.5
8	Network Interface 2	4	0.3

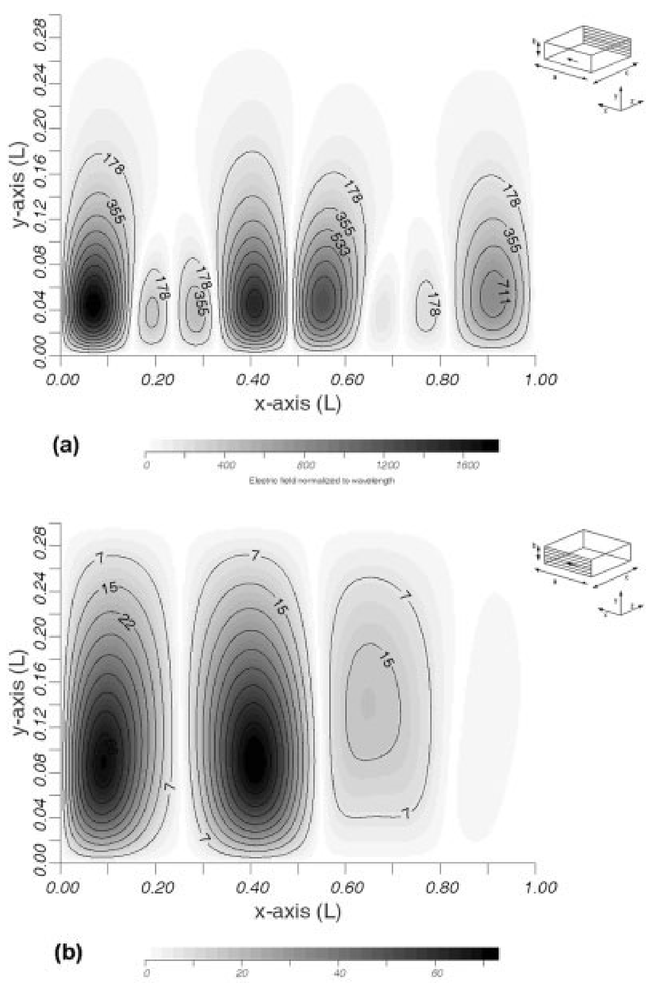

Figure 4 Electric field induced (a) on wall 1 and (b) on wall 4, by electric dipoles parallel to x-axis for $L = 0.1\lambda$

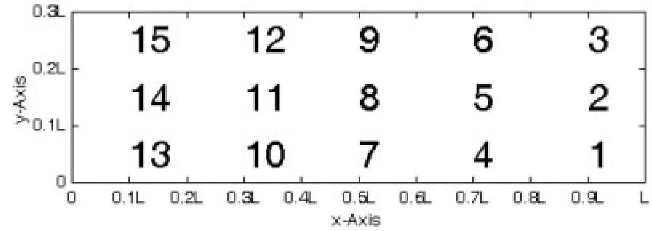

Figure 5 Wall points on walls of interest

4(a) and 4(b), respectively. It is clear that the higher field values are on wall 1 while the field values on wall 4 are even two orders of magnitude lower. This is expected, as more sources are closer to wall 1 than to wall 4. On both walls, the higher field values are at the left part of the wall. In all cases, there are areas on the walls where the electric field has small or near zero values. These areas would be the most suitable for creating holes and openings on the enclosure.

4. MONTE CARLO SIMULATION

The deterministic values calculated for the mapping matrix elements are accurate enough only if all the source characteristics (magnitude, polarization, and phase) are modeled correctly. The accurate prediction of electromagnetic emission from multiple source systems is a difficult or even impossible task due to their complexities. Therefore, a stochastic approach like Monte Carlo simulation can be applied. Such an approach has the advantage of proving a quantification of the major trends in a multiple-source system. Monte Carlo simulation has been applied successfully in many different engineering problems [28]. Monte Carlo simulations that are based on probability distributions describing source existence can give a first approximation of the emission level margins and perform a worst-case analysis.

The Monte Carlo Simulation procedure consists of three steps:

4.1. Step 1: Mapping Matrix Calculation

The mapping matrices are evaluated using the closed form expressions given in Section 2.

4.2. Step 2: Loop Process

A loop is performed with an adequate number of iterations. During the loop process, a random set of sources is generated according to a known probabilistic distribution [29]. All the elements ρ_{ij} of the mapping matrix are multiplied by a Bernoulli random variable ζ_i that lies in the set of values [0, 1] and represents the existence or not of source i. Therefore, the result is a new matrix A′ [18] with elements $\rho_{ij}\zeta_i$. The direction of the dipole sources may vary using phase binomial distributions with 0° or 180° phase difference between the dipoles. Then, the random variable ζ_i is given by[b]

$$\zeta_i = \zeta_{ie}\zeta_{ip}, \tag{7}$$

where ζ_{ie} is the random variable of the source existence distribution, and ζ_{ip} is the random variable of the phase distribution. Matrix A′ is calculated for every iteration.

4.3. Step 3: Statistical Processing of the Results

After the end of the Monte Carlo simulation the statistical processing begins. The wall points with the highest probability of peak electric field values are found. The statistical analysis of the results involves the calculation of the 90th percentile values. The 90th percentile gives the value below of which lie the 90% of the samples.

Monte Carlo simulation using both source existence and phase binomial distributions was applied on the source model presented in the previous section. The electric field values are calculated for 15 different wall points inside the cavity. The positions of these wall points are given in Figure 5. All source amplitudes are assumed equal to each other.

5. SOURCE PLACEMENT PROBLEM DEFINITION

A PCB designer is always interested in finding the appropriate source placement that reduces the EMI levels. Therefore an optimization method must be employed to find the optimum positions of the sources inside the board. The objective of the optimization procedure presented in this work is to reduce the electric field values at the bottom of the opposite walls 1 and 4 (see Fig. 1), assuming that openings will be created at these positions. The electric field at these positions is reduced by minimizing a specific mathematical expression, called fitness function and given by:

$$f = \sum_{1}^{N}\left(\sum_{1}^{M}\left|E^{\mathrm{Wall1}}\right| + \left|E^{\mathrm{Wall4}}\right|\right) \tag{8}$$

where N is the number of the sources, M is the number of the wall points chosen at the bottom of walls 1 and 4, and E^{Wall1}, E^{Wall4} are the electric field values on walls 1 and 4, respectively. The variables of the fitness function are the x and z coordinates of the sources. All the sources are assumed to be in the same y-plane $y' = 0.05L$. The only possible moves of the sources within each distinct area are along x and z-axis (y coordinates remain unchanged). The sources in the RAM area are allowed to move only along z axis. The initial grid is that of Figure 3.

Two different evolutionary optimization algorithms were applied to the above-described problem. We use a steady state GA with parallel populations [30] and PRSA [23]. GAs have been applied in a variety of electromagnetic engineering problems [22]. PRSA is described in the next subsection.

5.1. Parallel Recombinative Simulated Annealing

Parallel recombinative simulated annealing (PRSA) is a hybrid method that inherits the parallelism property and the population concept, including recombination operators, from GAs, and the property of convergence from simulated annealing. The fundamentals of PRSA can be found in [23]. The basic structure of PRSA is similar to that of a genetic algorithm. Thus, PRSA generates new individuals by applying crossover and mutation operators, and every new population is created by selection from old (parents) and new (children) individuals. The difference from normal genetic algorithms is that the selection process is based on Boltzmann trials, which are controlled by a parameter T called temperature, just like in simulated annealing method.

The criterion used to determine whether the new individual is accepted or rejected is called "Metropolis criterion" [23] and is based on the fitness assigned to individuals. As the fitness value is decreased, individuals are considered to be of better quality. According to the Metropolis criterion, if the fitness value of the child is less than the fitness of the parent, the child is accepted and replaces the parent in the next generation. Otherwise, the child replaces the parent with probability exp{[fitness (parent) − fitness (child)]/T} greater than a random number distributed uniformly in the interval [0, 1]. It is obvious that PRSA selections are mostly random when the temperature is high. In this case, the fitness value of an individual is not so important. As the temperature decreases, the degree of randomness goes down and selection depends increasingly on the fitness of the individual. The temperature is decremented according to the expression

$$T_{\text{new}} = \text{CF} \times T_{\text{old}} \tag{9}$$

where CF is a positive parameter, less than unity, called "cooling factor." Cooling down slowly (CF close to 1) gives better solutions, although the algorithm takes longer to converge. Therefore, in this work, CF is considered equal to 0.9.

The selection strategy is very important in PRSA because it refers to which individuals are chosen to form the next generation. Therefore, parents and children have to compete against each other to prevail. There are three types of competition:

1. Every child competes against one of its own two parents.
2. Every child competes against one random parent in the current generation.
3. Parents and children compete in reverse order of their fitness values, i.e., the best child competes against the worst parent in the current generation, the second-best child against the second-worst parent, etc.

Regarding solution quality, the first selection strategy "child against own parent" was proved in [25] to be the best one, and thus this strategy is adopted in our work.

PRSA is inherently an algorithm best suited for parallel and distributed computer systems although a version that runs in a single computer also exists. In this case individuals migrate from one node to another at certain intervals. The number of individuals that migrate from any node is controlled by a specific parameter called "migration rate." In brief, the parallel version of the PRSA algorithm can be described by the following steps:

FOR each node of the computer system DO in parallel:

1. Set T to a sufficiently high value.
2. Initialize the population (generate NP random individuals).
3. Calculate the fitness of each individual.
4. REPEAT
   i. Mark all individuals as "unused."
   ii. Do NP/2 times:
      (a) Select randomly two "unused" individuals (parents).
      (b) Generate two new individuals (children) by applying crossover operator.
      (c) Apply mutation operator to each child.
      (d) Calculate the fitness of each child.
      (e) Select two individuals from the two parents and the two children by applying the Boltzmann trial.
      (f) Mark winning individuals as "used" and replace the two parents with those individuals.
   iii. Periodically lower T according to expression [9].
   iv. Select individuals for migration and send them to other nodes.
   v. Receive new individuals from other nodes. Replace the individuals sent before with received individuals.
5. UNTIL termination criterion is satisfied.

To keep the subpopulation size (number of individuals kept by a node) constant, the migration rate must be fixed for all nodes. When individuals are sent to a node, they are buffered until that node has finished sending. Then, they replace the individuals sent by that node and the buffer is cleared. It was shown in [25] that

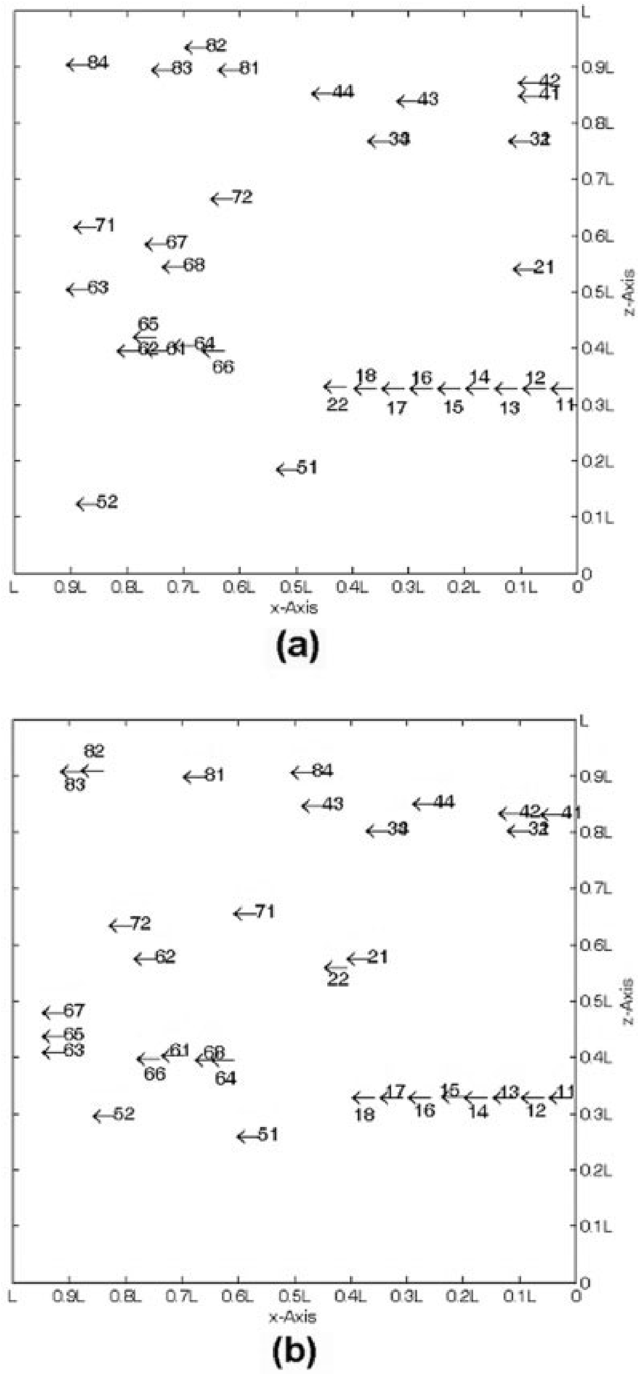

Figure 6 Telecommunications equipment source grids optimized by (a) GA and (b) PRSA

solution quality decreases if more than one-fourth of a subpopulation migrates. In this work, the migration rate is set equal to 25% of the subpopulation size.

The migration strategy is very important in parallel PRSA because it refers to which individuals are selected to migrate to other nodes. Two types of migration are suggested:

1. Every node chooses the best individuals and sends them to the neighbor nodes.
2. Every node chooses randomly individuals and sends them to the neighbor nodes.

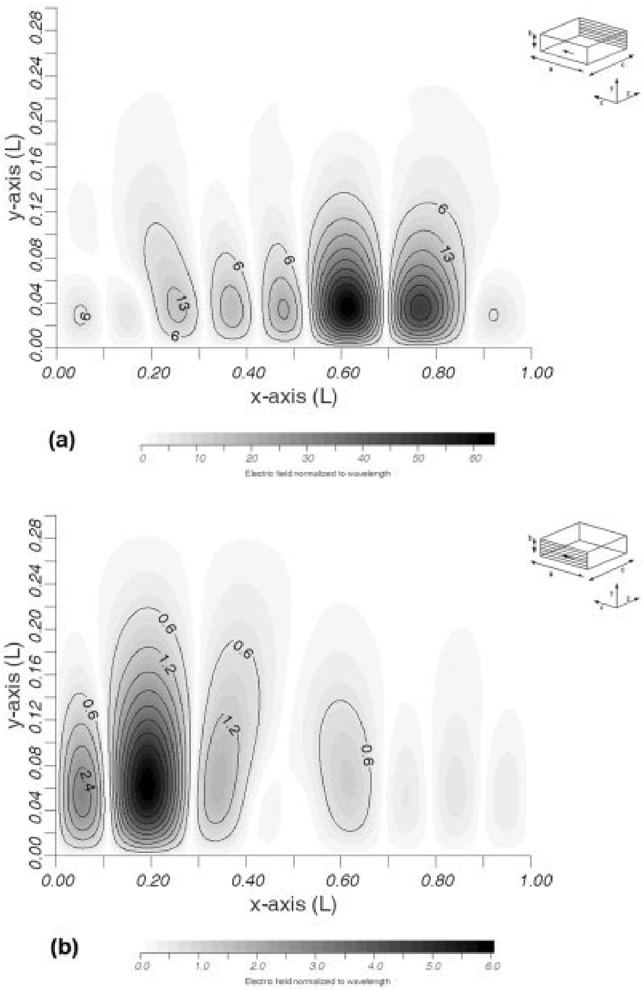

Figure 7 Source grid optimized by GA. Electric field induced (a) on wall 1 and (b) on wall 4, by electric dipoles parallel to x-axis for $L = 0.1\lambda$

Regarding the computation time, the first migration strategy "choose best" was proved in [25] to be faster, and thus this strategy is adopted in our work.

5.2. Optimization Results

We allow both algorithms to run for 20 times and we select the best results. For both algorithms, the population size is set to 100, and the number of parallel populations is 5. The crossover and the mutation probability are set to 0.9 and 0.01, respectively. The migration rate is set to 25% and the "choose best" migration strategy is applied. Both algorithms run for 5000 generations. For PRSA, the cooling constant was set to 0.9 and the temperature drops in every generation. The initial temperature is set to 100,000, and the final is set to 0.1. We have used a parallel implementation running in five different PCs using parallel virtual machine (PVM) [31].

The optimized grids found by both methods are shown in Figures 6 (a) and 6(b). The electric field on walls 1 and 4 is computed for the resulting source configurations. Figures 7 (a), 7(b), 8 (a), and 8(b) show the values of the electric field for the GA and the PRSA computed grids, respectively. One may notice that these values are more than one order of a magnitude less than the electric field values derived by the initial grid for both walls. The PRSA grid seems to perform better than the GA one.

To validate if these specific source configurations reduce the induced field, Monte Carlo simulation should also be applied. Monte Carlo simulation is a stochastic approach able to show if random source configurations of these source placements produce in average lower electric field values than the initial grid. We apply both source existence and phase difference binomial distributions. The source existence probability is different in each board area as shown in Table 1. The phase change probability is set to 0.5 for all areas. The statistical quantity examined here is the 90th percentile. A comparison of the Monte Carlo results of the 90th percentile for the initial and the optimized grids for walls 1 and 4 is shown in Figures 9(a) and 9(b). The optimized grids reduce the electric field up to an order of magnitude in the worst case for wall 1. For wall 4, both GA and PRSA perform satisfactory giving values smaller than or equal to the initial ones. It is obvious that the results derived by the PRSA algorithm give the smaller field values on both walls. These results indicate that the Monte Carlo technique, combined with evolutionary optimization methods, can be useful in predicting and reducing emission level margins.

6. CONCLUSIONS

In this work, a framework has been presented that combines evolutionary optimization algorithms with stochastic procedures to suppress EMI inside metallic enclosures of telecommunications equipment. A generic model of telecommunications equipment has

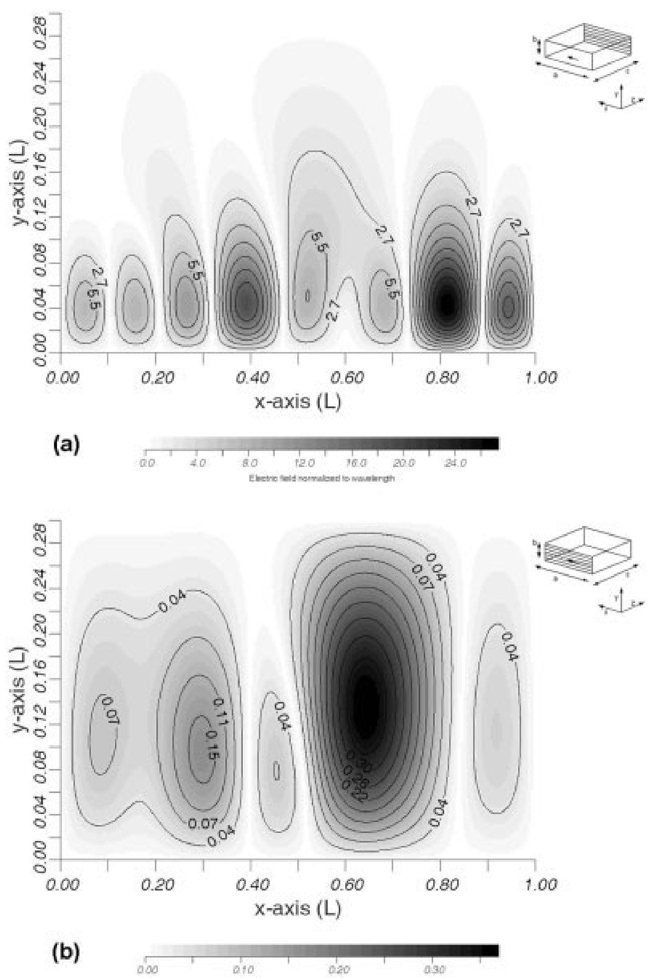

Figure 8 Source grid optimized by PRSA. Electric field induced (a) on wall 1 and (b) on wall 4, by electric dipoles parallel to x-axis for $L = 0.1\lambda$

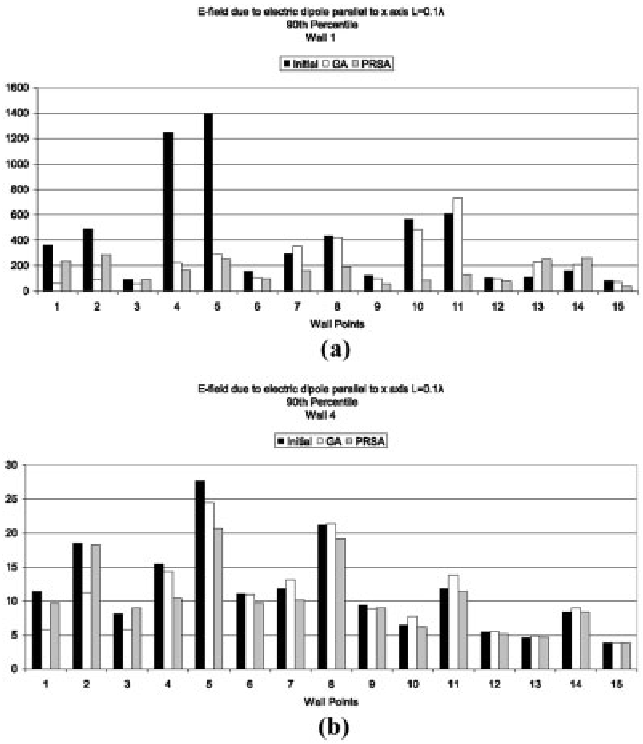

Figure 9 Ninetieth percentile electric field values (a) for wall 1 and (b) for wall 4. The electric dipoles have 50% probability of phase change

been created based on observations on several types of wired and wireless devices. It is observed that usually such a device has sources placed in asymmetrical positions in distinct areas. Two different evolutionary algorithms have been applied for the reduction of the electric field at the bottom of two opposite walls. It is found that PRSA outer performs a parallel GA with the same population size. Monte Carlo simulation has also been used to perform a worst-case analysis. Similar methods can be applied to a variety of equipment. Telecommunications equipment manufacturers can easily apply these techniques to make early risk limiting decisions during a PCB design process.

REFERENCES

1. K. Chang, RF and Microwave Wireless Systems, Wiley, New York 2000.
2. K. Chang, I. Bahl, and V. Nair, RF and microwave circuit and component design for wireless systems, Wiley, New York, 2002.
3. K. Chang, Handbook of RF/microwave components and engineering, Wiley, Hoboken, NJ, 2003.
4. C.R. Paul, Introduction to electromagnetic compatibility, Wiley, New York, 1980.
5. S. Ramo, J.R. Whinnery, and T. Van Duzer, Fields and waves in communication electronics, 2nd ed., Wiley, New York, 1984.
6. Y. Jeong, J. Kim, J.H. Kwon, and J. Kim, Analytical calculation of radiated emissions from rectangular power bus using embedded capacitor in high-speed packages and PCBs, Microwave Opt Technol Lett 48 (2006), 358-361.
7. S. Haga, K. Nakano, T. Sudo, and O. Hashimoto, Study on reduction in radiated emissions from PCB using test LSI, Microwave Opt Technol Lett 36 (2003), 238-242.
8. L.C. Fung, S.W. Leung, and L. Wan, A model for crosstalk prediction in PCB layout, Microwave Opt Technol Lett 30 (2001), 142-144.
9. R. Azaro, S. Caorsi, M. Cosso, G.M. Costini, M. Donelli, R. Ene, G.L. Gragnani, and M. Pastorino, A semianalytical approach for the evaluation of radiated immunity on a printed-circuit board in metallic enclosures, Microwave Opt Technol Lett 27 (2000), 204-207.
10. K.Y. See and J.-G. Ma, Electromagnetic radiation from printed-circuit structure with extended conductor, Microwave Opt Technol Lett 27 (2000), 118-120.
11. R. Peña-Rivero, H.J. Aguilar, and R. Linares y Miranda, Optimum use of high-impedance surface in PCB to mitigate the simultaneous switching noise and radiated emission, Microwave Opt Technol Lett 48 (2006), 1446-1449.
12. C. Feng and Z. Shen, Shielding effectiveness of a metallic enclosure with multiple apertures, Microwave Opt Technol Lett 43 (2004), 447-450.
13. W. Chamma, S. Kashyap, and A. Louie, Electromagnetic penetration into a cavity with a slot, Microwave Opt Technol Lett 25 (2000), 175-181.
14. J. Carlsson and I. Belov, Influence of a slot on the induced current in a wire inside a conducting box with a square aperture, Microwave Opt Technol Lett 32 (2002), 25-29.
15. R. Azaro, S. Caorsi, M. Donelli, and G. L. Gragnani, Evaluation of the effects of an external incident electromagnetic wave on metallic enclosures with rectangular apertures, Microwave Opt Technol Lett 28 (2001), 289-293.
16. C.-T. Tai and P. Rozenfeld, Different representations of dyadic Green's functions for a rectangular cavity, IEEE Trans Microwave Theory Tech 24 (1976), 597-601.
17. R. Crawhall, EMI potential of multiple sources within a shielded enclosure, Doctoral Thesis, University of Ottawa, Ottawa, 1993.
18. S.K. Goudos, E. Vafiadis, and J.N. Sahalos, Monte Carlo simulation for the prediction of the emission level from multiple sources inside shielded enclosures, IEEE Trans Electromagn C 44 (2002), 291-308.
19. S. Goudos, T. Samaras, E. Vafiadis, and J.N. Sahalos, Numerical approaches for EMI reduction of ICs and PCBs inside metallic enclosures, Proc 2003 IEEE Int Symp Electromagn C 1 (2003), 513-516.
20. R.R. Goulette, The measurement of radiated emissions from integrated circuits, Proc IEEE Int Symp Electromagn C 1992, 340-345.
21. F.R. Cooray, R. Crawhall, and G.I. Costache, Radiated fields from circuit components inside rectangular enclosures with apertures, Canad J Electrical Comput Eng 16 (1991), 143-147.
22. Y. Rahmat-Samii and E. Michielssen, Electromagnetic optimization by genetic algorithms, Wiley, New York, 1999.
23. S.W. Mahfoud and D.E. Goldberg, Parallel recombinative simulated annealing: A genetic algorithm, Parallel Comput 21 (1995), 1-28.
24. K. Kurbel and A. Ruppel, Integrating intelligent job-scheduling into a real-world production-scheduling system, J Intell Manuf 7 (1996), 373-377.
25. K. Kurbel, B. Schneider, and K. Singh, Solving optimization problems by parallel recombinative simulated annealing on a parallel computer—An application to standard cell placement in VLSI design, IEEE Trans Systems Man Cybern B Cybern 28 (1998), 454-461.
26. S. Fei and K. Chakrabarty, Unified high-level synthesis and module placement for defect-tolerant microfluidic biochips, Proc 42nd Des Autom Conf 2005, 825-830.
27. S.K. Goudos and C.S. Hilas, Numerical modeling and measurements of radiated emissions from integrated circuits inside telecommunications equipment, WSEAS Trans Commun 6 (2007), 499-504.
28. R.Y. Rubinstein, Simulation and the Monte Carlo method, Wiley, New York, 2001.
29. A. Papoulis, Probability, random variables and stochastic processes, 2nd ed., McGraw-Hill Series in Electrical Engineering, New York, 1984.
30. M. Wall, GAlib: A C++ library of genetic algorithm components, Version 2.4, Document Revision B, MIT Press, Cambridge, MA, 1996.
31. A. Geist et al., PVM: Parallel Virtual Machine, A users' guide and tutorial for networked parallel computing, MIT Press, Cambridge, MA, 1994. Available: http://www.netlib.org/pvm3/book/nodel7.html.